© S. Hirzel Verlag · EAA
acta acustica · ACUSTICA
Vol. 87 (2001) 322–332

Transient Processes Near the Acoustic Threshold of Parametrically-Driven Bubble Shape Oscillations

A. O. Maksimov

Pacific Oceanological Institute, Far East Branch of Russian Academy of Sciences, 43, Baltic Street, Vladivostok 690041, Russia

T. G. Leighton

Institute of Sound and Vibration Research, University of Southampton, Highfield, Southampton SO17 1BJ, United Kingdom

Summary
The nonlinear response of a gas bubble to a low frequency ω_p pumping wave results in parametrically-generated shape oscillations above a well-defined threshold. This may be detected through insonification of the bubble by a high-frequency ω_i imaging wave, leading to the scattering of signals at $\omega_i \pm \omega_p$, $\omega_i \pm \omega_p/2$ (corresponding to pulsation and subharmonic wall oscillation, respectively). The durations of the transient regimes of these two signals are very different. In this study the complete theory of the transient processes near the threshold of excitation of distortion modes has been derived. The growth of an instability is very slow in this domain, causing the transient processes associated with establishing steady state surface oscillations to be of very long duration.

PACS no. 43.25.Ts, 43.25.Yw

1. Introduction

Non-spherical oscillations of gas bubbles in acoustic fields have been the subject of numerous investigations [1, 2, 3, 4, 5, 6, 7, 8, 9, 10, 11, 12]. It is known from experiments that these surface oscillations arise as a bifurcation from the basic purely radial oscillatory motion. They occur in liquids of relatively low viscosity when the amplitude of the driving (or pump) acoustic field exceeds a threshold. The shape distortion is greatest when the pump signal (of angular frequency ω_p) is tuned to the resonance of the bubble under investigation. Under these conditions the frequency σ_l of the parametrically excited surface waves approaches half the frequency of the breathing mode [10, 13]. This resonance would however be limited by damping due to acoustical reradiation, thermal diffusion and viscous losses associated with the breathing mode, and viscous damping of distortion modes. A major success in recent theoretical studies has been a realization of the importance of coupling between the radial and the shape modes [14, 15, 16, 17]. These results are reviewed in depth in [18].

Surface oscillations are readily detected by observing relatively large bubbles visually [19, 3, 20] or by a modification of the method of interferometry [21, 22].

Another manifestation of surface waves has been observed by Leighton *et al.* [23] by the use of a two frequency technique, when in addition to a pumping wave the bubble is insonified by a high frequency imaging wave. For applications with millimeter- sized bubbles, the pumping frequency is of kilohertz order, whilst the imaging frequency is usually around a megahertz. Because of the great difference between the timescales associated with these two fields, the slow shape oscillations of the bubble wall (having frequency $\omega_p/2$) will modulate the scattering imaging wave. The wavelength of the imaging wave is comparable with the bubble size. Because of this, the higher partial components ($l > 1$), corresponding to the expansion of the imaging wave of angular momentum l, will be scattered effectively by shape oscillations with wavelengths $\sim R/l$. As a result, they will give rise to spectral components that are comparable with those associated with scattering by the breathing mode[1] [24, 25].

More recently, Ramble *et al.* [26] have discovered that there exists a significant difference in the transient times taken to establish steady-state subharmonic and fundamental combination frequency signals (the so-called "ring-up" times). The primary objective of this paper is to explain this difference.

The approach is as follows. A phase space analysis of the system is made, where "fixed points" (corresponding to the equilibrium positions from which the system will not deviate if unperturbed) are identified. The character of these fixed points (attractor, repulsor, or saddle) is determined by the signs of the real parts of the eigenvalues. Since these eigenvalues reflect the rates of change of the parameter in linear independent directions in phase space, they can be identified with the damping (uniform negative values of the real parts being required, for example, for an attractor). The

Received 29 September 2000,
accepted 3 April 2001.

[1] The spherical harmonic expansion coefficients of the scattering amplitude $f(\theta, \alpha)$ are named partial amplitudes (partial components) $f(\theta, \alpha) = \sum f_{lm} Y_{lm}(\theta, \alpha)$. The incoming plane imaging wave can also be expanded in spherical harmonics. The scattering matrix $S(l, m|l_1 m_1)$ determines the effectiveness of transformation from incoming partial components to scattering partial components e.g. - the effectiveness of scattering. When the imaging wave is scattered by the breathing mode (at $k_i R_0 \sim 1$), the scattering of some first partial components $l \sim 0, 1, 2$ will be effective. In contrast, scattering by the distortion modes will be effective for higher partial amplitudes $l \sim 8, 9, 10$, as the corresponding wavelength of the surface modes R_0/l will be smaller than $\lambda_i = 2\pi/k_i$. As a result the angular dependence of the radiation of the combinative component ($\omega_i \pm \omega_p$) should differ markedly from that of the subharmonic component ($\omega_i \pm \omega_p/2$).

eigenvalues can be determined in the space close to each fixed point through a linearised analysis.

The explanation proposed here for the difference in the ring-up times of subharmonic and fundamental combination frequency signals, relies on the fact that these measurements were made slightly above the threshold of excitation of the distortion mode [26]. In this domain, one of the eigenvalues of the linear stability problem λ_1 is small and positive (it equals zero at the threshold, which would be likened to zero damping).

Full consideration is here given to the problem of parametrically driven distortion modes, accounting for all spherical harmonics. With one exception [9], papers on this subject have discussed only those spherical harmonics Y_{l0} which exhibit axial symmetry [4, 5, 6, 8, 10, 11, 12, 13, 14, 18, 25]. However the environment around the bubble, and the long-wavelength pumping field, are isentropic. Since no unique direction is distinguished, inclusion of only the axially symmetric spherical harmonics is inadequate. All spherical harmonics corresponding to $(2l+1)$-fold degenerate resonant frequency σ_l should give comparable contributions to the overall oscillations.

2. Parametric generation of surface waves

Consider an air filled bubble of radius R driven by a pumping wave of amplitude P_m and angular frequency ω_p in the absence of an imaging wave. The water compressibility can be ignored in the limit of $R_0\omega_p/c_0 \ll 1$ [9] and the velocity potential, denoted by ϕ, is governed by

$$\Delta\phi = 0, \qquad \boldsymbol{v} = \nabla\phi, \tag{1}$$
$$P = -\rho_0\left[\dot{\phi} + (\nabla\phi)^2/2\right] + P_\infty + P_m\sin(\omega_p t),$$

where $\boldsymbol{v}$ is the velocity and P is the pressure in liquid, ρ_0 and P_∞ are the equilibrium density and pressure, and P_m is the amplitude of pumping wave. We shall use the spherical coordinates (r,θ,α) and write the equation of the bubble surface as $r = R_0 + \xi(\theta,\alpha,t)$. Then the kinematic boundary condition takes the form

$$\left[\frac{\partial}{\partial t} + (\boldsymbol{v},\nabla)\right](r-R)_{r=R_0+\xi} = 0. \tag{2}$$

The dynamic boundary condition is that the pressure on the two sides of the surface differ only because of surface tension i.e. if P_l and P_g denote the pressure in the water and in the bubble respectively, then

$$P_l = P_g - \frac{\sigma}{\rho_0}(\nabla,\boldsymbol{n}), \quad P_g = P_0(V_0/V)^\gamma, \tag{3}$$

where $\boldsymbol{n}$ is the unit vector normal to the surface $r = R_0 + \xi(\theta,\alpha,t)$; σ is the coefficient of surface tension. We adopt a polytropic law for the gas in the bubble and V, V_0 are the instantaneous and equilibrium bubble volume, γ is the polytropic exponent, P_0 is the equilibrium pressure in the bubble.

We express $\boldsymbol{v}$ and P through the velocity potential ϕ, and write down the kinematic (4) and dynamic (5) boundary conditions in a form which is correct to second order in (ξ/R_0) [9, 10, 13]:

$$\frac{\partial\xi}{\partial t} - \frac{\partial\phi}{\partial r} = \frac{\partial^2\phi}{\partial r^2}\xi - \frac{1}{R_0^2}\left(\frac{\partial\xi}{\partial\theta}\frac{\partial\phi}{\partial\theta}\right) - \frac{1}{\sin^2\theta R_0^2}\left(\frac{\partial\xi}{\partial\alpha}\frac{\partial\phi}{\partial\alpha}\right) \quad (r = R_0), \tag{4}$$

$$\frac{\partial\phi}{\partial t} + \frac{\sigma}{\rho_0 R_0^2}(2+\nabla_s^2)\xi - R_0\omega_0^2\bar{\xi} = -\xi\frac{\partial^2\phi}{\partial t\partial r} - \frac{1}{2}\left(\frac{\partial\phi}{\partial r}\right)^2 - \frac{1}{2R_0^2}\left[\left(\frac{\partial\phi}{\partial\theta}\right)^2 + \frac{1}{\sin^2\theta}\left(\frac{\partial\phi}{\partial\alpha}\right)^2\right] + \frac{2\sigma}{\rho_0 R_0^3}\xi(1+\nabla_s^2)\xi + \omega_0^2\left[\overline{\xi^2} - 3/2(\gamma+1)\bar{\xi}^2\right] - \frac{P_m\sin(\omega_p t)}{\rho_0} \quad (r = R_0), \tag{5}$$

where $\omega_0^2 = 3\gamma P_0/\rho_0 R_0^2$ is the frequency of the fundamental (breathing) mode, ∇_s^2 is the surface Laplacian, and the spherical average of ξ is defined by

$$\bar{\xi} = \frac{1}{4\pi}\int_0^{2\pi} d\alpha \int_0^{\pi} \xi(\theta,\alpha)\sin\theta\, d\theta.$$

Equations (4) and (5) are distinguished from those of Mei and Zhou [13] by terms accounting for the dependence of ξ, ϕ on the polar angle α.

Using the isentropic nature of the problem we expand ξ and ϕ in terms of the spherical harmonics

$$\xi = \sum_{l=0}^{\infty}\sum_{m=-l}^{m=l}\xi_{lm}(t)Y_{lm}(\theta,\alpha),$$
$$\phi = \sum_{l=0}^{\infty}\sum_{m=-l}^{m=l}\phi_{lm}(t)\left(\frac{R_0}{r}\right)^{l+1}Y_{lm}(\theta,\alpha),$$
$$Y_{lm}(\theta,\alpha) = (-1)^m\sqrt{\frac{2l+1}{4\pi}\frac{(l-m)!}{(l+m)!}}P_l^m(\cos\theta)e^{im\alpha} \quad (m \geq 0),$$
$$Y_{l-m} = (-1)^m Y_{lm}^*, \tag{6}$$

where P_l^m denotes the associated Legendre polynomial and $Y_{l-m} = (-1)^m Y_{lm}^*$, $(m \geq 0)$. The spherical harmonics are normalized such that

$$\int_0^{2\pi} d\alpha \int_0^{\pi} \sin\theta\, d\theta\, Y_{lm}^* Y_{lm} = 1,$$

and $\xi_{00} = \bar{\xi}\sqrt{4\pi}$. The displacement and potential are real, so that $\xi = \xi^*$, $\phi = \phi^*$ (here an asterisk denotes the complex conjugation). These conditions lead to definite relations between the components of expansion of the Legendre polynomial of $\xi_{lm} = (-1)^m\xi_{l-m}^*$, $\phi_{lm} = (-1)^m\phi_{l-m}^*$. On substituting equation (6) into equations (4) and (5) we obtain

$$\frac{\partial\xi_{lm}}{\partial t} + \frac{l+1}{R_0}\phi_{lm} = \sum_{l_1 m_1}\sum_{l_2 m_2}\xi_{l_1 m_1}\phi_{l_2 m_2}\delta_{m,m_1+m_2}$$

acta acustica · ACUSTICA
Vol. 87 (2001)

$$\cdot \frac{1}{R_0^2}\Big[(l_2+1)(l_2+2)\Big\langle lm\Big|Y_{l_1m_1}\Big|l_2m_2\Big\rangle - \Big\langle lm\Big|\frac{\partial Y_{l_1m_1}}{\partial\theta}\frac{\partial}{\partial\theta}\Big|l_2m_2\Big\rangle + m_1m_2\Big\langle lm\Big|\frac{Y_{l_1m_1}}{\sin^2\theta}\Big|l_2m_2\Big\rangle\Big], \quad (7)$$

$$\frac{\partial\phi_{lm}}{\partial t} - \frac{\sigma}{\rho_0 R_0^2}(l-1)(l+2)\xi_{lm} - R_0\omega_0^2\bar{\xi}\sqrt{4\pi}\delta_{lm,00} = -\frac{P_m}{\rho_0}\sin(\omega_p t)\sqrt{4\pi}\delta_{lm,00} + \Bigg\{\sum_{l_1m_1}\sum_{l_2m_2}\xi_{l_1m_1}\dot{\phi}_{l_2m_2}\delta_{m,m_1+m_2}\cdot\frac{l_2+1}{R_0}\Big\langle lm\Big|Y_{l_1m_1}\Big|l_2m_2\Big\rangle - \sum_{l_1m_1}\sum_{l_2m_2}\phi_{l_1m_1}\phi_{l_2m_2}\delta_{m,m_1+m_2}\cdot\frac{1}{R_0^2}\Big[\frac{(l_2+1)(l_2+2)}{2}\Big\langle lm\Big|Y_{l_1m_1}\Big|l_2m_2\Big\rangle + \Big\langle lm\Big|\frac{\partial Y_{l_1m_1}}{\partial\theta}\frac{\partial}{\partial\theta}\Big|l_2m_2\Big\rangle - m_1m_2\Big\langle lm\Big|\frac{Y_{l_1m_1}}{\sin^2\theta}\Big|l_2m_2\Big\rangle\Big] - \frac{2\sigma}{\rho_0 R_0^2}\sum_{l_1m_1}\sum_{l_2m_2}\xi_{l_1m_1}\xi_{l_2m_2}\delta_{m,m_1+m_2}\cdot\Big[(l_2+1)l_2-1\Big]\Big\langle lm\Big|Y_{l_1m_1}\Big|l_2m_2\Big\rangle + \omega_0^2\Big[\overline{\xi^2} - 3/2(\gamma+1)\bar{\xi}^2\Big]\sqrt{4\pi}\delta_{lm,00}\Bigg\}, \quad (8)$$

where the following notation for the matrix elements of operators has been used

$$\Big\langle lm\Big|\hat{F}\Big|l_2m_2\Big\rangle \equiv \int_0^{2\pi}\mathrm{d}\alpha\int_0^{\pi}\sin\theta\,\mathrm{d}\theta\,Y_{lm}^*\hat{F}Y_{l_2m_2}.$$

We find to first order approximation

$$\frac{\partial\xi_{00}^{(1)}}{\partial t} + \frac{1}{R_0}\phi_{00}^{(1)} = 0,$$
$$\frac{\partial\phi_{00}^{(1)}}{\partial t} - R_0\omega_*^2\xi_{00}^{(1)} = 0, \quad (9a)$$
$$\frac{\partial\xi_{lm}^{(1)}}{\partial t} + \frac{l+1}{R_0}\phi_{lm0}^{(1)} = 0,$$
$$\frac{\partial\phi_{lm}^{(1)}}{\partial t} - \frac{\sigma(l-1)(l-2)}{\rho_0 R_0^3}\xi_{lm}^{(1)} = 0 \quad (l>0). \quad (9b)$$

Homogeneous solutions satisfying (9a,b) consist of a shape preserving (breathing) mode and shape distorting (surface) modes

$$\xi_{00}^{(1)} = \frac{1}{2}\Big(a_{00}\mathrm{e}^{\mathrm{i}\omega_* t} + a_{00}^*\mathrm{e}^{-\mathrm{i}\omega_* t}\Big), \quad (10a)$$
$$\phi_{00}^{(1)} = -\frac{1}{2}\mathrm{i}\omega_*\Big(a_{00}\mathrm{e}^{\mathrm{i}\omega_* t} - a_{00}^*\mathrm{e}^{-\mathrm{i}\omega_* t}\Big);$$

$$\xi_{lm}^{(1)} = \frac{1}{2}\Big(a_{lm}\mathrm{e}^{\mathrm{i}\sigma_l t} + b_{lm}\mathrm{e}^{-\mathrm{i}\sigma_l t}\Big), \quad (10b)$$
$$\phi_{lm}^{(1)} = -\frac{1}{2}\mathrm{i}\frac{\sigma R_0}{l+1}\Big(a_{lm}\mathrm{e}^{\mathrm{i}\sigma_l t} - b_{lm}\mathrm{e}^{-\mathrm{i}\sigma_l t}\Big);$$
$$\omega_*^2 = \omega_0^2 - 2\sigma/\rho_0 R_0^3,$$
$$\sigma_l^2 = \frac{\sigma}{\rho R_0^3}(l-1)(l+1)(l+2),$$
$$b_{lm} = (-1)^m a_{l-m}^*.$$

We shall analyze the case of the near resonant interaction between the breathing and distortion modes: $\omega_* \approx 2\sigma_l + \Delta\omega(R_0)$, $|\Delta\omega| \ll \omega_*$. Here $\Delta\omega(R_0)$ denotes the frequency mismatch for a given R_0. The definition of amplitudes given here differs from the one used by Mei and Zhou [13] by a co-factor 1/2, thus providing more physical sense of a_{00} and a_{lm}.

The evolution equations for the complex amplitudes a_{lm} result from the conditions under which the secular forcing terms vanish in the second order equations [13]. We omit these cumbersome calculations, as the procedure is straightforward and well known. The final result is

$$\frac{\partial}{\partial t}\Big(\frac{a_{00}}{\sqrt{4\pi}}\Big) = \mathrm{i}Q_0^l\mathrm{e}^{\mathrm{i}(2\sigma_l-\omega_*)t}\sum_{m=-l}^{l}(-1)^m a_{lm}a_{l-m} + \frac{P_m\sqrt{\pi}}{2\omega_*\rho_0 R_0}\mathrm{e}^{\mathrm{i}(\omega_p-\omega_*)t}, \quad (11)$$
$$\frac{\partial a_{lm}}{\partial t} = \mathrm{i}Q_l^0\mathrm{e}^{\mathrm{i}(\omega_*-2\sigma_l)t}(-1)^m\Big(\frac{a_{00}}{\sqrt{4\pi}}\Big)a_{l-m}^*,$$

where we define

$$Q_0^l = \frac{(4l-1)\sigma_l}{64\pi(l+1)R_0},$$
$$Q_l^0 = \frac{(4l-1)\sigma_l}{4R_0}.$$

Expansion of the bubble wall displacement and the potential over the normalized set Y_{lm} (see equation 6) leads to different normalization factors (constants) in the definition of amplitudes a_{lm} and coefficients Q_l^0 and Q_0^l from those obtained when non-normalized associated Legendre polinomials $P_l \sim Y_{l0}$ are used [9, 10, 13]. For example, the radial component of bubble wall displacement is equal to $\Delta R = \xi_{00}Y_{00} = \xi_{00}(1/\sqrt{4\pi})$ and thus the amplitude of radial pulsation (see 10a) is $a_{00}/\sqrt{4\pi}$. Accounting for damping and converting system equations (11) to an autonomous one by the transformation

$$a_{00} = \tilde{a}_{00}\mathrm{e}^{\mathrm{i}(\omega_p-\omega_*)t},$$
$$a_{lm} = \tilde{a}_{lm}\mathrm{e}^{\mathrm{i}(\omega_p/2-\omega_l)t},$$

we get the desired evolution equations

$$\frac{\partial}{\partial t}\Big(\frac{\tilde{a}_{00}}{\sqrt{4\pi}}\Big) = \mathrm{i}(\omega_*-\omega_p)\Big(\frac{\tilde{a}_{00}}{\sqrt{4\pi}}\Big) - \gamma_0\Big(\frac{\tilde{a}_{00}}{\sqrt{4\pi}}\Big) + \mathrm{i}Q_0^l\sum_{m=-l}^{l}(-1)^m\tilde{a}_{lm}\tilde{a}_{l-m} + \frac{P_m}{2\omega_*\rho_0 R_0}, \quad (12a)$$

$$\frac{\partial \tilde{a}_{lm}}{\partial t} = \mathrm{i}(\sigma_l - \omega_p/2)\tilde{a}_{lm} - \gamma_l \tilde{a}_{lm} + (-1)^m \mathrm{i} Q_l^0 \left(\frac{\tilde{a}_{00}}{\sqrt{4\pi}}\right) \tilde{a}^*_{l-m}, \quad (12b)$$

$$\gamma_0 = \frac{1}{2}(k_p R_0)\omega_p + \frac{2\nu}{R_0^2} + 3(\gamma - 1)\frac{\omega_p}{R_0}\sqrt{\frac{2D}{\omega_p}},$$

$$\gamma_l = (l+2)(2l+1)\frac{\nu}{R_0^2}.$$

Here γ_0 is the sum of radiation damping, viscous damping and damping due to thermal diffusion for the breathing mode; γ_l is the viscous damping of the l-th distortion mode, as estimated by a linear analysis. These equations reduce[2] to the expressions derived by earlier investigators [13, 25], when one retains only the axi-symmetric ($m = 0$) modes.

3. Steady state solutions

To use the stationary solutions of the evolution equations derived by Mei and Zhou, we introduce collective variables for the description of the distortion modes:

$$S = \sum_{m=-l}^{l} (-1)^m \tilde{a}_{lm}\tilde{a}_{l-m}, \quad N = \sum_{m=-l}^{l} (-1)^m \tilde{a}_{lm}\tilde{a}^*_{lm}.$$

The governing equations for S and N follow immediately from equation (12b).

$$\dot{N} = -2\gamma_l N + \mathrm{i} Q_l^0 \left[\left(\frac{\tilde{a}_{00}}{\sqrt{4\pi}}\right) S^* - \left(\frac{\tilde{a}_{00}}{\sqrt{4\pi}}\right)^* S\right], \quad (13)$$

$$\dot{S} = 2\left[\mathrm{i}(\sigma_l - \omega_p/2) - \gamma_l\right] S + 2\mathrm{i} Q_l^0 \left(\frac{\tilde{a}_{00}}{\sqrt{4\pi}}\right) N,$$

$$\frac{\partial}{\partial t}\left(\frac{\tilde{a}_{00}}{\sqrt{4\pi}}\right) = \left[\mathrm{i}(\omega_* - \omega_p) - \gamma_0\right]\left(\frac{\tilde{a}_{00}}{\sqrt{4\pi}}\right) + \mathrm{i} Q_0^l S + \frac{P_m}{2\omega_* \rho_0 R_0}.$$

The stationary states are realized when the right hand sides of equations (13) become zero. This dynamical system of fifth order for N, U, V, x, y ($S = U + \mathrm{i}V$, $\tilde{a}_{00}/\sqrt{4\pi} = x + \mathrm{i}y$) has the following fixed points:

$$N_1 = 0, \quad U_1 = 0, \quad V_1 = 0;$$

$$x_1 = \frac{P_m}{2\omega_* \rho_0 R_0}\frac{\gamma_0}{(\omega_* - \omega_p)^2 + \gamma_0^2},$$

$$y_1 = \frac{P_m}{2\omega_* \rho_0 R_0}\frac{\omega_* - \omega_p}{(\omega_* - \omega_p)^2 + \gamma_0^2}.$$

This means that purely radial oscillations can occur. The nature of the solution trajectories is determined by a linear stability analysis. The corresponding five eigenvalues are:

$$\lambda_{1,2} = -\gamma_l \pm \sqrt{Q_l^{*2}(x_1^2 + y_1^2) - (\sigma_l - \omega_p/2)^2},$$
$$\lambda_3 = -2\gamma_l; \qquad \lambda_{4,5} = -\gamma_0 \pm \mathrm{i}(\omega_* - \omega_p), \quad (14)$$

where the convention is that λ_1 given by the positive root and λ_2 by the negative one etc. Any small perturbation of shape will remain small – i.e. the purely radial oscillation is stable, when all real parts of the eigenvalues are negative. The eigenvalue λ_1 can change its sign, and thus this fixed point (i) is transformed into a saddle point. The condition under which λ_1 vanishes determines the threshold of instability of distortion modes:

$$Q_l^{0\,2}(x_1^2 + y_1^2) = (\sigma_l - \omega_p/2)^2 + \gamma_l^2. \quad (15)$$

Another two fixed points (ii) and (iii) are given by the following expressions

$$N_{2,3} = \frac{1}{Q_0^l Q_l^0}\left[(\sigma_l - \omega_p/2)(\omega_* - \omega_p/2) - \gamma_l\gamma_0\right] \pm \left(\left[(\sigma_l - \omega_p/2)(\omega_* - \omega_p/2) - \gamma_l\gamma_0\right]^2 + \left(\frac{P_m Q_l^0}{2\omega_* \rho_0 R_0}\right)^2 - \left[(\sigma_l - \omega_p/2)^2 + \gamma_l^2\right]\left[(\omega_* - \omega_p)^2 + \gamma_0^2\right]\right)^{1/2}$$

$$N_{2,3}^2 = U_{2,3}^2 + V_{2,3}^2, \qquad U_{2,3} = N_{2,3}\cos\theta_{2,3},$$

$$V_{2,3} = N_{2,3}\sin\theta_{2,3}, \qquad \sin\theta_2 = -\sin\theta_3,$$

$$x_{2,3} = \frac{\gamma_l}{Q_l^0}\sin\theta_{2,3} - \frac{\sigma_l - \omega_p/2}{Q_l^0}\cos\theta_{2,3},$$

$$y_{2,3} = -\frac{\sigma_l - \omega_p/2}{Q_l^0}\sin\theta_{2,3} - \frac{\gamma_l}{Q_l^0}\cos\theta_{2,3},$$

$$\cos\theta_{2,3} = -\frac{\gamma_l(\sigma_l - \omega_p/2) + \gamma_0(\omega_* - \omega_p)}{P_m Q_0^l/2\omega_* \rho_0 R_0}. \quad (16)$$

The linearized stability of these fixed points leads to an eigenvalue problem given by an algebraic equation of fifth order. Note that $\lambda_3 = -4\gamma_l$ is the solution that is the same for fixed points (ii) and (iii). The expressions for the remaining eigenvalues (four for fixed point (ii) and four for fixed point (iii)) can be obtained in closed form but are very cumbersome. However, since we are interested only in whether these fixed points are stable or unstable, and how this stability is affected as the control parameters are varied, it is possible to use simpler arguments.

Consider a bifurcation diagram in the plane of the control parameters $(\omega_p/2\pi)$, P_m (see Figure 1). The curve L_{th} is the threshold of instability of the fixed point (i), described by (15). This state is unstable ($\Re e\lambda_1 > 0$) above this curve and is stable ($\Re e\lambda_1 < 0$) below it. The plot is made of an air bubble in water of equilibrium radius 1.19 mm. This is the case studied experimentally by Ramble *et al.* [26], who measured the growth of surface waves at $P_m = 50$ Pa on a bubble having a breathing-mode resonance of 2.7 kHz. A horizontal line

[2] Because of the normalization and definition adopted (10a,b) the partitional amplitudes differ from those found by previous workers [9, 10, 11]. To obtain agreement one should simultaneously change the sign and the value of the coefficient Q and sign of $\Delta\omega$.

acta acustica · ACUSTICA
Vol. 87 (2001)

on Figure 1 indicates this amplitude. The figure shows that for this bubble the lowest threshold for parametric excitation of surface waves corresponds to the modes with $l = 11$. Following values of damping are adopted $\gamma_0/\omega_* = 0.0126$, $\gamma_{11}]/\omega_* = 0.0171$ (see [27]). For comparison the threshold for the nearest resonance with $l = 12$ modes is shown by a dashed line.

If the fixed points are hyperbolic (i.e., none of eigenvalues lie on imaginary axis), varying of control parameters does not change the nature and the stability of the fixed points, since the hyperbolic points are structurally stable [28]. The fixed point (i) is hyperbolic on the plane of control parameters with the exception of the curve L_{th}. The fixed points (i) and (ii) coalesce at the values of control parameters on the branches of the curve L_{th} between the points F_+, F_-. The states realized when the control parameters take the values corresponding to the points F_+, F_- are critical. Here the confluence of all fixed points (i), (ii), (iii) takes place. The points $F_\pm$ occur at frequencies $f_\pm$ such that:

$$2\pi f_\pm = (\sigma_l + \omega_*/2) \pm \sqrt{(\sigma_l - \omega_*/2)^2 + 2\gamma_0\gamma_l},$$

$$\frac{(P_l)_\pm Q_l^0}{2\rho\omega_* R_0} = \pm\Big[\gamma_l(\sigma_l - \omega_p/2) + \gamma_0(\omega_* - \omega_p)\Big].$$

The fixed points (i) and (iii) coalesce on the branches of the curve L_{th} located at the higher points F_+, F_-. The fixed points (ii) and (iii) coalesce on the lines $L_\pm$, where:

$$\frac{P_l Q_l^0}{2\rho\omega_* R_0} = \pm\Big[\gamma_l(\sigma_l - \omega_p/2) + \gamma_0(\omega_* - \omega_p)\Big]. \qquad (17)$$

The point of intersection of these lines (L_+, L_-) is given by:

$$P_m = 0, \quad \omega_b = \omega_*\left[1 - \frac{1 - 2\sigma_l/\omega_*}{1 - 2\gamma_0/\gamma_l}\right].$$

The fixed points (ii) and (iii) are nonhyperbolic only on these lines and on the corresponding branches of the curve L_{th}, where confluence takes place.

In this paper we shall analyze only the neighborhood of the threshold of the generation of distortion modes, that is, the neighborhood of the branch of the bifurcation curve L_{th} located between the points F_+, F_-. In this case the fixed point (ii) has a single zero eigenvalue with the remaining eigenvalues having negative real parts. Below the threshold the fixed point (i) is stable and (ii) is unstable. These two fixed points coalesce at the threshold, and above the threshold (i) is unstable and (ii) is stable. Thus, an exchange of stability has occurred at the threshold. This type of bifurcation is called a transcritical bifurcation [28].

Notice that N, by definition, is a sum of the squares of $(2l + 1)$ amplitudes and thus is positive. States (ii) and (iii) are physical only if $N_2, N_3 \geq 0$. This condition leads to the following classification.

The only stable state (i) exists in the domain below the lines $L_\pm$ (lightly shaded and labeled (A) in the figure). Another domain in Figure 1 (darkly shaded and labeled (B) lies above the lines L_+, L_-, but below the threshold (below the curve L_{th}). In this, there is a stable state (i) and two unphysical states (ii) and (iii), as N_2 and N_3 are negative. In domain (C), above the threshold L_{th}, state (i) is unstable. The corresponding fixed point is a saddle, N_2 is positive, but N_3 is negative and thus it corresponds to an unphysical state. State (ii) describes the steady state amplitude of the collective variables of distortion modes given by (16). The final domains (D) are located between the lines L_+, L_- and the curve L_{th}. Here state (i) is stable, and N_2 and N_3 are positive.

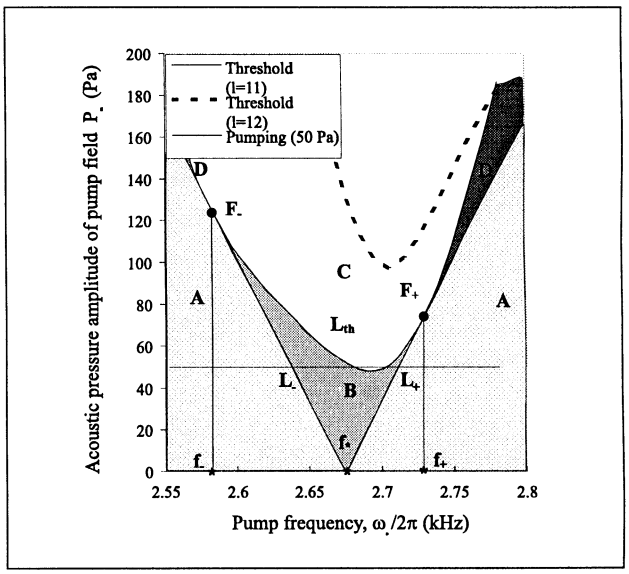

Figure 1. The control space for the acoustic pressure amplitude (P_m) and frequency ($\omega/2\pi$) of the pump field, as relating to an air bubble of equilibrium radius 1.19 mm in water under 1 atmosphere. The bifurcation curves for parametrically driven shape oscillations ($l = 11$, solid curve; $l = 12$, dashed curve) are shown. The neighbouring threshold curve for $l = 10$ does not fit on this graph: its minimum occurs at a frequency of 2.70 kHz and takes a value of 220 Pa. Hence the figure shows the threshold curve which gives the lowest minimum of these three is $l = 11$ (giving 49 Pa at 2.69 kHz.) A horizontal line indicates a pump field amplitude of 50 Pa. Points F_+, F_-, lines L_+, L_- and domains A–D, are discussed in the text.

Having identified the regions of instability of surface waves, the transient regime will now be examined in that region to determine how rapidly the instability will develop.

4. Transient regime

The solution of the system equations (13) is based on the use of the master-slave principle [29] known in applied mathematics as center-manifold reduction [28]. Near the point where the dynamical system equations (13) loses its linear stability (in our case this occurs at the threshold), one can reduce the dimentionality of the system and exclude the stable (fast) variables (i.e. those which decay to central manifold on timescales determined by the corresponding eigenvalues λ_2, λ_3, λ_4, λ_5). Thus, if we are interested in long-time behavior, we need only to investigate the system restricted to the central manifold which is determined by a relatively simple equation

for the parameter of order (using Landau terminology) that varies "slowly" (i.e. on time scales comparable with. $1/\lambda_1$).

As the first step we transform the linear part of equation (13) into block diagonal form.

The new coordinates in phase space (η, μ, ζ) correspond to the eigenvectors of eigenvalues $(\lambda_1, \lambda_2, \lambda_3)$ respectively.

$$\begin{aligned}
\eta &= N + \frac{x_1(\sigma_1 - \omega_p/2) - y_1 Rd}{Q_l^0(x_1^2 + y_1^2)} U \\
&\quad + \frac{y_1(\sigma_1 - \omega_p/2) + x_1 Rd}{Q_l^0(x_1^2 + y_1^2)} V, \\
\mu &= N + \frac{x_1(\sigma_1 - \omega_p/2) + y_1 Rd}{Q_l^0(x_1^2 + y_1^2)} U \\
&\quad + \frac{y_1(\sigma_1 - \omega_p/2) - x_1 Rd}{Q_l^0(x_1^2 + y_1^2)} V, \\
\zeta &= (\sigma_1 - \omega_p/2)N + x_1 Q_l^0 U + y_1 Q_l^0 V, \\
Rd &= \sqrt{Q_l^{0^2}(x_1^2 + y_1^2) - (\sigma_1 - \omega_p/2)^2}. \qquad (18)
\end{aligned}$$

Differentiating equations (18) by t and expressing derivations of N, U, V by use equation (13), we obtain

$$\begin{aligned}
\frac{\partial \eta}{\partial t} &= \lambda_1 \eta - 2Q_l^0 \big(yU(\eta,\mu,\zeta) - xV(\eta,\mu,\zeta)\big) \\
&\quad - 2Q_l^0 N(\eta,\mu,\zeta) \\
&\quad \cdot \left(y \frac{x_1(\sigma_1 - \omega_p/2) - y_1 Rd}{Q_l^0(x_1^2 + y_1^2)} \right. \\
&\quad \left. - x \frac{y_1(\sigma_1 - \omega_p/2) + x_1 Rd}{Q_l^0(x_1^2 + y_1^2)}\right) \qquad (19a) \\
\frac{\partial \mu}{\partial t} &= \lambda_2 \xi - 2Q_l^0 \big(yU(\eta,\mu,\zeta) - xV(\eta,\mu,\zeta)\big) \\
&\quad - 2Q_l^0 N(\eta,\mu,\zeta) \\
&\quad \cdot \left(y \frac{x_1(\sigma_1 - \omega_p/2) + y_1 Rd}{Q_l^0(x_1^2 + y_1^2)} \right. \\
&\quad \left. - x \frac{y_1(\sigma_1 - \omega_p/2) - x_1 Rd}{Q_l^0(x_1^2 + y_1^2)}\right) \qquad (19b) \\
\frac{\partial \zeta}{\partial t} &= \lambda_3 \zeta - 2Q_l^0(\sigma_1 - \omega_p/2) \\
&\quad \cdot \big(yU(\eta,\mu,\zeta) - xV(\eta,\mu,\zeta)\big) \\
&\quad - 2Q_l^0 N(\eta,\mu,\zeta)(x_1 y - y_1 x), \qquad (19c) \\
\frac{\partial x}{\partial t} &= -\gamma_0(x - x_1) - (\omega_* - \omega_p)(y - y_1) \\
&\quad - Q_0^l V(\eta,\mu,\zeta), \qquad (19d) \\
\frac{\partial y}{\partial t} &= -(\omega_* - \omega_p)(x - x_1) - \gamma_0(y - y_1) \\
&\quad - Q_0^l U(\eta,\mu,\zeta). \qquad (19e)
\end{aligned}$$

Here N, U, and V are expressed in terms of η, μ, ζ by inversion of transformation (18).

The relaxation of the variables μ, ζ, x, y is fast compared with η. Thus one can find local equilibrium values of μ, ζ, x, y (depending on η) from the conditions under which the right hand sides of (19b,c,d,e) vanish. Substituting these values in (19a) we get the desired self-consistent equation for the parameter of order η.

Resolving the equations for x, y we get

$$\begin{aligned}
(x - x_1) &= -\frac{Q_0^l\big[(\omega_* - \omega_p)U + \gamma_0 V\big]}{(\omega_* - \omega_p)^2 + \gamma_0^2}, \\
(y - y_1) &= -\frac{Q_0^l\big[\gamma_0 U - (\omega_* - \omega_p)V\big]}{(\omega_* - \omega_p)^2 + \gamma_0^2}. \qquad (20)
\end{aligned}$$

On substitution of equation (20) into the right hand sides of equations (19) one can see that in the main order of magnitude $\mu, \zeta \approx 0$. The first non-vanishing contribution arises only in the second order $\mu, \zeta \sim \eta^2$. Further simplifications arise from neglecting the deviation from the threshold in all terms excluding λ_1.

$$\begin{aligned}
\lambda_1 &\approx \frac{(P_m Q_l^0/2\omega_*\rho_0 R_0)^2}{\gamma_l\big[(\omega_* - \omega_p)^2 + \gamma_0^2\big]} \\
&\quad - \Big[(\sigma_l - \omega_p/2)^2 + \gamma_l^2\Big]\frac{1}{\gamma_l}. \qquad (21)
\end{aligned}$$

As a result, the system equations (19) leads to the desired equation for the parameter of order

$$\begin{aligned}
\frac{\partial \eta}{\partial t} &= \left\{\Big(P_m Q_l^0/2\omega_*\rho_0 R_0\Big)^2 \right. \qquad (22) \\
&\quad \left. - \Big[(\sigma_l - \omega_p/2)^2 + \gamma_l^2\Big]\Big[(\omega_* - \omega_p)^2 + \gamma_0^2\Big]\right\}\frac{\eta}{\gamma_l} \\
&\quad - Q_l^0 Q_0^l\Big[(\omega_* - \omega_p)(\sigma_l - \omega_p/2)^2 - \gamma_0\gamma_l\Big] \\
&\quad \cdot \Big[(\sigma_l - \omega_p/2)^2 + \gamma_l^2\Big]\gamma_l^{-3}\Big[(\omega_* - \omega_p)^2 + \gamma_0^2\Big]^{-1}\eta^2,
\end{aligned}$$

with

$$\begin{aligned}
N &\approx \frac{(\sigma_l - \omega_p/2)^2 + \gamma_l^2}{2\gamma_l^2}\eta, \\
U &\approx -\frac{P_m Q_l^0}{2\omega_*\rho_0 R_0}\frac{\big[(\omega_* - \omega_p)\gamma_l + (\sigma_l - \omega_p/2)\gamma_0\big]}{2\gamma_l^2\big[(\omega_* - \omega_p)^2 + \gamma_0^2\big]}\eta, \\
V &\approx -\frac{P_m Q_l^0}{2\omega_*\rho_0 R_0}\frac{\big[(\omega_* - \omega_p)(\sigma_l - \omega_p/2) - \gamma_l\gamma_0\big]}{2\gamma_l^2\big[(\omega_* - \omega_p)^2 + \gamma_0^2\big]}\eta.
\end{aligned}$$

For the accuracy adopted one can use N as a parameter of order, as it has more direct physical sense - the sum of the squares of amplitudes of the resonant distortion modes (that is the sum of occupation numbers of these modes). Introducing an approximate expression for N_2 equation (16) near the threshold:

$$\begin{aligned}
N_2 &\approx -\Big[(P_m Q_l^0/2\omega_*\rho_0 R_0)^2 \qquad (23) \\
&\quad - \big[(\sigma_l - \omega_p/2)^2 + \gamma_l^2\big]\big[(\omega_* - \omega_p)^2 + \gamma_0^2\big]\Big] \\
&\quad \cdot \Big[2Q_l^0 Q_0^l\big[(\omega_* - \omega_p)(\sigma_l - \omega_p/2)^2 - \gamma_0\gamma_l\big]\Big]^{-1}
\end{aligned}$$

we get the final result

$$\frac{\partial N}{\partial t} = \lambda_1 N\left(1 - \frac{N}{N_2}\right). \qquad (24)$$

Here λ_1 and N_2 are given by equation (21) and equation (23) correspondingly. The range of applicability of equation (24)

acta acustica · ACUSTICA
Vol. 87 (2001)

is the neighborhood of the threshold, but not too close to the critical points F_+, F_-, where there are two zero eigenvalues (co-dimension two points). The reason is that equations (4), (5), and (7) are only correct to second order in nonlinear terms. Near the critical points F_+, F_- the coefficient before N_2 in equation (24) (λ_1/N_2) is small (it equals zero at critical points) and one should account for the terms of third order, but that would be exceeding the accuracy of the initial equations.

The solution of equation (24) has the form

$$N(t) = \frac{N(0)N_2}{N(0)\left[1 - \mathrm{e}^{-\lambda_1 t}\right] + N_2 e^{-\lambda_1 t}}, \qquad (25)$$

where $N(0)$ is the initial value. As equation(25) is only valid at times greater than the damping of the unforced breathing γ_0^{-1} and distortion γ_l^{-1} modes, the physical sense of $N(0)$ is the characteristic value of the sum of the squares of amplitudes (occupation numbers) of the resonant distortion modes at times, $(\gamma_0^{-1}, \gamma_1^{-1}) \ll t \ll \lambda_1^{-1}$. For the conditions of the experiment [26] $(\omega_p/2\pi) = 2700\,\mathrm{Hz}$ and adopted values of damping $(\gamma_0/\omega_*) = 0.0126$, $(\gamma_{11}/\omega_*) = 0.0171$; $\gamma_0^{-1} \approx 4.6 \cdot 10^{-3}\,\mathrm{s}$, $\gamma_{11}^{-1} \approx 3.4 \cdot 10^{-3}\,\mathrm{s}$. At greater times $t \gg \lambda_1^{-1}$, $N(t)$ approaches N_2 asymptotically. One should note that the parametric resonant excitation (unlike the ordinary resonance) requires the presence of initial distortions - there is no unstable rise of the state $N(0) = 0$. These distortions comprise natural fluctuations or are stipulated by the excitation of surface modes at the onset of insonification. The time to establish the steady state of the slow degree of freedom of the distortion modes $\sim \lambda_1^{-1} \ln(N_2/N(0))$ - will greatly exceed the corresponding time for the fast degrees of freedom γ_0^{-1}. This discrepancy will be determined not only by the smallness of $(\gamma_0/\lambda)^{-1}$ but by the greatness of $\ln(N_2/N(0))$.

Now we shall discuss the transient regime for the breathing mode. According to equation (16), the steady state amplitude of the breathing mode above the threshold does not depend on the pump field acoustic pressure (see also [13, 16, 18]):

$$\frac{\left|\tilde{a}_{00}(\infty)\right|^2}{4\pi} = x(\infty)^2 + y(\infty)^2 = x_2^2 + y_2^2 = \left[(\sigma_l - \omega_p/2)^2 + \gamma_l^2\right]/Q_l^{0\,2}.$$

This can be seen in more detail by expressing x_1 and y_1 in terms of N by use of equations (21) and (25). The square of the amplitude of the breathing mode is found to be

$$\frac{\left|\tilde{a}_{00}(\infty)\right|^2}{4\pi} = x_1^2 + y_1^2 + \frac{2Q_0^l\left[(\omega_* - \omega_p)(\sigma_l - \omega_p/2) - \gamma_0\gamma_l\right]}{\left[(\omega_* - \omega_p)^2 + \gamma_0^2\right]Q_l^0} N(t).$$

Here we retain only those terms which are linear in N. Since N tends to N_2 which is proportional to the deviation from the threshold, one should recognize that the terms are of the same order in calculating x_1, y_1. This gives

$$\frac{\left|\tilde{a}_{00}(\infty)\right|^2}{4\pi} = \frac{(\sigma_l - \omega_p/2)^2 + \gamma_l^2}{Q_l^{0\,2}} + \frac{2Q_0^l\left[(\omega_* - \omega_p)(\sigma_l - \omega_p/2) - \gamma_0\gamma_l\right]}{\left[(\omega_* - \omega_p)^2 + \gamma_0^2\right]Q_l^0} \cdot \left(N(t) - N_2\right). \qquad (26)$$

This result shows that the steady state amplitude of the breathing mode does not exceed its value at the threshold as predicted. This amplitude grows during the characteristic time γ_0^{-1} until reaching a maximum magnitude. It then decreases slowly until it attains the steady state level, parametrically exciting distortion modes.

We have examined the problem of nonlinear bubble shape oscillations in terms of collective variables. Finding the evolution of the breathing mode permits us to analyze the dynamics of $(2l + 1)$ resonant distortion modes.

5. Standing surface waves

We shall find the solution of equation (12b) on the time scale $t \gg \gamma_l^{-1}$ when the parametric forcing term is a known function of time. Equation (12b) describes the parametric interaction of breathing mode with "progressive surface waves" having equatorial wavenumbers m, and propagating eastwards $(m > 0)$ or westward $(m < 0)$ around the sphere. We pass from the complex amplitudes $\tilde{a}_m$, $\tilde{a}_{-m}$ to the real amplitudes and phases $\tilde{a}_m = \sqrt{N_m}\exp(\mathrm{i}\psi_m)$, $\tilde{a}_{-m} = \sqrt{N_m}\exp(\mathrm{i}\psi_{-m})$. In terms of these variables, equation (12b) is represented as follows:

$$\dot{N}_m = -2\gamma_l N_m + 2(-1)^m Q_l^0 \frac{|\tilde{a}_{00}|}{\sqrt{4\pi}} \cdot \sqrt{N_m N_{-m}} \sin\left((\psi_m + \psi_{-m}) - \arg(\tilde{a}_{00})\right), \qquad (27a)$$

$$\dot{N}_{-m} = -2\gamma_l N_{-m} + 2(-1)^{-m} Q_l^0 \frac{|\tilde{a}_{00}|}{\sqrt{4\pi}} \cdot \sqrt{N_m N_{-m}} \sin\left((\psi_m + \psi_{-m}) - \arg(\tilde{a}_{00})\right), \qquad (27b)$$

$$\dot{\psi}_m = (\sigma_l - \omega_p/2) + 2(-1)^m Q_l^0 \frac{|\tilde{a}_{00}|}{\sqrt{4\pi}} \cdot \sqrt{\frac{N_{-m}}{N_m}} \cos\left((\psi_m + \psi_{-m}) - \arg(\tilde{a}_{00})\right), \qquad (27c)$$

$$\dot{\psi}_{-m} = (\sigma_l - \omega_p/2) + 2(-1)^{-m} Q_l^0 \frac{|\tilde{a}_{00}|}{\sqrt{4\pi}} \cdot \sqrt{\frac{N_m}{N_{-m}}} \cos\left((\psi_m + \psi_{-m}) - \arg(\tilde{a}_{00})\right), \qquad (27d)$$

With N_m, N_{-m} given by the equations (27a,b) we find

$$\frac{\partial}{\partial t}\left(N_m - N_{-m}\right) = -2\gamma_l\left(N_m - N_{-m}\right).$$

It follows from this equation that over a short time interval (within the timescale under consideration, i.e. λ_1^{-1}) the amplitudes of waves encountered with the same equatorial wave number m will be equal. Similarly, from the equations (27c,d) one gets

$$\frac{\partial}{\partial t}\left(\psi_m - \psi_{-m}\right) \approx 0, \qquad (28)$$

which means that the phase difference between these two waves will be approximately constant, and equal to the phase difference when the waves are initially set up. This initial phase difference is accidental by its nature as it is stipulated by fluctuations. It will now be shown that the sum of the phases is a fast variable which reaches its local equilibrium value, depending on the slow variable $N(t)$, over the characteristic time γ_l^{-1}. On substituting $N_m \approx N_{-m}$ into equations (27), summation of equations (27c) and (27d) gives

$$\frac{\partial}{\partial t}\Big(\psi_m - \psi_{-m}\Big) = 2(\sigma_l - \omega_p/2) \tag{29}$$
$$+ (-1)^{-m} 2Q_l^0 \frac{|\tilde{a}_{00}|}{\sqrt{4\pi}} \cos\big((\psi_m + \psi_{-m}) - \arg(\tilde{a}_{00})\big).$$

To facilitate the solution, we use the derived expressions for the amplitude and the phase of the breathing mode and neglect small terms proportional to $N(t)$, N_2. In this approximation, equation (29) takes the form of an equation with constant coefficients and it can be integrated immediately. The solution decays exponentially to a stationary one as $t \gg \gamma_l^{-1}$ to give

$$\cos\big((\psi_m + \psi_{-m}) - \arg(\tilde{a}_{00})\big) \longrightarrow \frac{(-1)^{m+1}(\sigma_l - \omega_p/2)\sqrt{4\pi}}{Q_l^0 |\tilde{a}_{00}|}, \tag{30}$$
$$(-1)^m \sin\big((\psi_m + \psi_{-m}) - \arg(\tilde{a}_{00})\big) > 0.$$

One should note, that unlike condition (28), expression (30) leads to synchronization between the sum of the phase of progressive surface waves and the phase of the breathing mode. Introducing the notation $\beta \equiv \arccos[-(\sigma_l - \omega_p/2)\sqrt{4\pi} Q_l^{0-1} |\tilde{a}_{00}|^{-1}]$ and recalling that the principal value of arccos is defined in the interval $[0, \pi]$ [30] we have $\psi_m + \psi_{-m} = \arg(\tilde{a}_{00}) + \beta + m\pi$. On the other hand equation (28) leads to $\psi_m - \psi_{-m} = \psi_m(0) - \psi_{-m}(0)$. Combining these equations we get

$$\psi_m = \frac{1}{2}\Big(\arg(\tilde{a}_{00}) + \beta + m\pi + \psi_m(0) - \psi_{-m}(0)\Big),$$
$$\psi_{-m} = \frac{1}{2}\Big(\arg(\tilde{a}_{00}) + \beta + m\pi + \psi_m(0) - \psi_{-m}(0)\Big).$$

By excluding the fast variables $\psi_m, \psi_{-m}, (N_m - N_{-m})$, and thus reducing the problem to one of studying of "occupation numbers" N_m, we have

$$\dot{N}_m = 2\left\{ -\gamma_l + \sqrt{Q_l^{0\,2} \frac{|\tilde{a}_{00}|}{\sqrt{4\pi}} - (\sigma_l - \omega_p/2)^2} \right\} N_m,$$
$$N_m(t) = N_m(0) \exp\left\{ 2 \int_0^t \mathrm{d}t \left[-\gamma_l + \sqrt{Q_l^{0\,2} \frac{|\tilde{a}_{00}|^2}{\sqrt{4\pi}} - (\sigma_l - \omega_p/2)^2} \right] \right\}. \tag{31}$$

Substituting equation (26) into the integral, and retaining only those terms which are linear in N, the integration can be carried out to give the following simple and expected result:

$$N_m(t) = \frac{N_m(0)}{N(0)} N(t). \tag{32}$$

Note that (32) implies that the amplitudes of the partial standing waves excited on the bubble wall are proportional to initial, parametrically unstable fluctuations $N_m(0)$. Therefore they can not form any regular patterns. Now the appearance these standing waves is addressed.

Substitution of the derived expressions for the amplitudes and phases in the expansion (6), and utilizing the definitions (10) and (12), gives

$$\xi = \frac{|\tilde{a}_{00}|}{\sqrt{4\pi}} \cos\big(\omega_p t + \arg(\tilde{a}_{00})\big) + \left[\sqrt{N_0} \sqrt{\frac{2l+1}{4\pi}} P_l(\cos\theta) + \sum_{m=1}^{l} 2\sqrt{N_m} \sqrt{\frac{(2l+1)(l-m)!}{4\pi(l+m)!}} P_l(\cos\theta) \cdot \cos\left[m\alpha + \frac{1}{2}(\psi_m()0) - \psi_{-m}(0)) + \frac{\pi m}{2} \right] \right] \cdot \cos\left[\frac{\omega_p}{2} t + \frac{1}{2}\big(\arg(\tilde{a}_{00}) + \beta\big) \right], \tag{33}$$

where we have distinguished the contributions from the breathing mode and the distortion axi-symmetric mode, and combined the terms with plus and minus m.

This result shows that the excited distortion modes form $(l+1)$ standing waves oscillating in synchronous fashion relative to the phase of the breathing mode. The sum of the squares of the amplitudes of the breathing modes $N(t)$ is a regular quantity. However, the relations between the amplitudes of different modes, as well as the relative phases with respect to the polar angle, are accidental depending on the initial fluctuations. The unstable growth of this distortion fluctuation due to the parametric interaction with the breathing mode leads to the steady state distribution of energy between the breathing and distortion modes (for the range of the control parameters under discussion).

6. Discussion

We have examined the important features of transient bubble oscillations near the threshold of excitation of the distortion modes. The amplitudes of the shape oscillations are not large in this range, and so visualization of the distortions is a difficult problem. For the conditions of the experiment [26] $P_m \approx 50\,\mathrm{Pa}$, the magnitude N_2 is too small to allow visualization of the angular structure.

Nevertheless these distortions can be easy registered by acoustical methods. As has been shown by Leighton *et al.* [23], the insonification of the bubble by a high frequency $\omega_i \gg \omega_p$ imaging signal leads to the reradiation of the combinative components $\omega_i \pm \omega_p, \omega_i \pm \omega_p/2$. The mechanism

acta acustica · ACUSTICA
Vol. 87 (2001)

of generation of the combination frequencies is rather simple. The imaging wave scatters on the absolutely soft bubble surface, the instantaneous position and shape of which are determined by the slow motion forcing of the pumping wave.

The reradiated pressure in the far field can be written as [25]

$$P_{ip}^{(1)}(\omega) = \frac{e^{ikr_b}}{r_b} f_{ip}^{(1)}(\omega - \omega_i - \omega_p),$$

$$f_{ip}^{(1)} = i\frac{\langle \tilde{a}_{00}\rangle_{\omega-\omega_i-\omega_p}}{\sqrt{4\pi}} \frac{P_{mi}}{R_0 k_i} \cdot \sum_{l=0}^{\infty} \frac{P_l\big(\cos(\boldsymbol{e}\boldsymbol{k}_i/k_i)\big)}{2\pi\big[H_{l+1/2}^{(1)}(k_i R_0)\big]^2}, \tag{34}$$

where $P_{ip}^{1)}(\omega)$ and $f_{ip}^{1)}$ are the Fourier components of the pressure and the amplitude radiated by the breathing mode, $H_{l+1/2}^{(1)}$ is the Hankel function of the first kind; k_i is the wave number of the imaging wave, $\boldsymbol{e}$ is the unit vector in the direction from the center of the bubble to the receiver and r_b is the distance between these points, equation (34) shows contribution from the band $\omega_i + \omega_p$.

The expression for the pressure component near the $\omega_i + \omega_p/2$ given by [25] should be modified, as it accounted only for the single axi-symmetric mode contribution ($m = 0$).

$$P_{ip}^{(2)}(\omega) = \frac{e^{ikr_b}}{r_b} f_{ip}^{(2)}(\omega - \omega_i - \omega_p/2),$$

$$f_{ip}^{(2)} = i \sum_{m=-l}^{l} \Big\langle \sqrt{N_m} e^{-i(1/2)(\arg(\tilde{a}_{00})+v)} \Big\rangle_{(\omega-\omega_i-\omega_p/2)} \cdot e^{i(1/2)(\psi_m - \psi_{-m} + i\pi m)} \frac{P_{mi}}{R_0 k_i}$$

$$\cdot \sum_{l'=0}^{\infty} \sum_{m'=-l'}^{l'} \sum_{l''=0}^{\infty} \sum_{m''=-l''}^{l''} \frac{2i^{(l''-1)} Y_{l'm}(\boldsymbol{e}) Y_{l''m''}^*(\boldsymbol{k}_i/k_i)}{H_{l'+1/2}^{(1)}(k_i R_0) H_{l''+1/2}^{(1)}(k_i R_0)} \cdot \Big\langle l'm' | Y_{lm} | l''m'' \Big\rangle. \tag{35}$$

Here the matrix element $\langle l'm'|Y_{lm}|l''m''\rangle$ is expressed in terms of Wigner"s 3j symbols. The absence of this co-factor in expression (35) of [25] is a misprint.

It is doubtful that one can noticeably simplify equations (34) and (35) as the wavelength of the imaging field is comparable with the bubble size. Nevertheless comparison with the experimental results of Ramble *et al.* [26] can be made. The data plotted in Figure 2 show the maximum amplitudes of the subharmonic and the fundamental combination frequency signals. The time is measured in cycles of the pumping wave. From equations (34) and (35), the time-dependency of these amplitudes during the ring-up period are described by $C_1|\tilde{a}_{00}(t)|/\sqrt{4\pi}$ - for the fundamental combination frequency signal; and $C_2\sqrt{N(t)}$ for the subharmonic combination signal, where C_1 and C_2 are constants. It is difficult to find explicit magnitudes of these constants from (34), (35). One should expect that C_2 should be $(2l + 1)$ times smaller than C_1 as there is no spatial coherence between partial surface modes. We will use them as adjustable parameters.

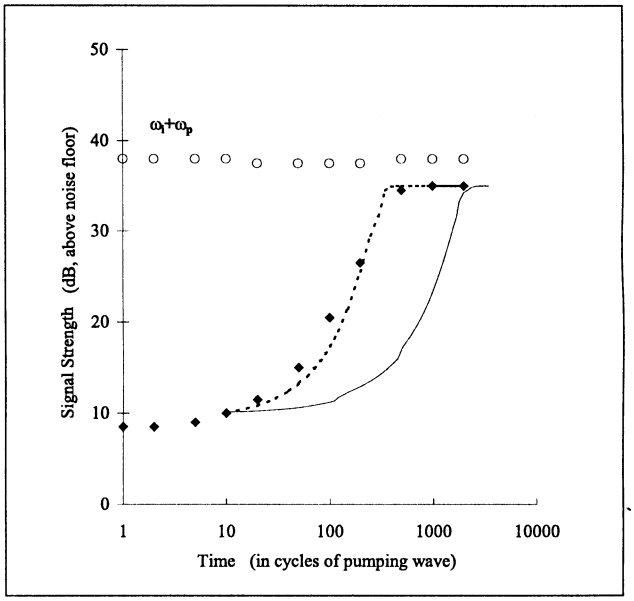

Figure 2. The comparison of experimental data on the transient regime of excitation of the fundamental o and the subharmonic • combinative components with the derived theoretical results: solid line - $\lambda_1 = 9 \cdot 10^{-4}\omega_*$, dashed line - $\lambda_1 = 6 \cdot 10^{-3}\omega_*$.

First, consider the fundamental combination frequency signal. For $|\tilde{a}_{00}(t)|^2$ given by equation (26), the values of the relevant coefficients must be chosen to correspond with the conditions of the experiment, specifically $P_m = 50\,\text{Pa}$, $(\omega_*/2\pi) = 2700\,\text{Hz}$, $(\gamma_0/\omega_*) = 0.0126$, $(\gamma_{11}/\omega_*) = 0.0171$. The frequency ratio (ω_p/ω_*) is set equal to 0.998. This is condition for which the numerical difference between the 50 Pa pump amplitude, and the threshold for generation of surface waves, takes the greatest positive value (Figure 1). The reasons for choosing this condition are discussed later. As a result, putting in values for the parameters in equation (26) we obtain

$$\frac{|\tilde{a}_{00}(t)|^2}{4\pi} = 2 \cdot 10^{-5} R_0^2 - 4 \cdot 10^{-3}\big(N(t) - N_2\big), \tag{36}$$

with N_2 given by equation (23) $N_2 = 2 \cdot 10^{-4} R_0^2$. Thus the variation of the fundamental combination frequency signal at the timescale λ_1^{-1} is negligibly small

$$\frac{|\tilde{a}_{00}(\infty)|^2 - |\tilde{a}_{00}(0)|^2}{|\tilde{a}_{00}(0)|^2} = \frac{4 \cdot 10^{-3}\big(N_2 - N(0)\big)}{2 \cdot 10^{-5} R_0^2 + 4 \cdot 10^{-3}\big(N_2 - N(0)\big)} \approx \frac{4 \cdot 10^{-3} N_2}{2 \cdot 10^{-5} R_0^2} = 4 \cdot 10^{-2},$$

$$\big(N_2 \gg N(0),\ N(\infty) = N_2\big)$$

in comparison with its value reached during the initial characteristic time γ_0^{-1}. This fact is in agreement with the experimental data plotted in Figure 2 where no noticeable variation of the fundamental combination frequency signal is observed at the timescale λ_1^{-1}. We use $C_1 = 2.2 \cdot 10^6 (P_N/R_0)$ to

adjust equation (36) to fit to the data located at $\sim$ 40 dB above the noise floor P_N.

To compare the subharmonic combination frequency signal, we must first find the magnitude of λ_1, given by equation (21). On substituting the accepted values for the parameters (see above), we obtain $\lambda_1 = 9 \cdot 10^{-4}\omega_*$. The specific problem arises in finding $N(0)$, contained in equation (25). It is reasonable to take it as $(2l + 1)$ times the square of the amplitude of shape oscillations corresponding to noise level P_N. However, as follows from the experimental data, the amplitude of the distortion mode increases by ten times from the noise level during a few periods. In the "master-slave" approximation employed, we cannot analyze the process on that small time scale, so we shall use $N(0)$ as an adjustable parameter. From the data point at ten periods we have $C_2 = 10(P_N/\sqrt{N(0)})$. We take the second condition for finding C_2 and $\sqrt{N(0)}$ from the steady state level of the combination signal $\sim$ 35 dB above the noise level. Thus $C_2 = 10^{3.5}(P_N/\sqrt{N_2})$ and eliminating C_2 we get $N(0) = 10^{-5}N_2$. It should be noted that the values derived for the adjustable parameters C_1, C_2 are not contradicting, as it was expected that $C_1/C_2 \sim 10$.

The transient regime of the subharmonic combination frequency component, calculated on the basis of equation (25), is plotted in Figure 2 as a solid line. This result shows that the theory derived here can explain the greatly increased time required to establish bubble shape oscillations. However there is quantitative disagreement between the predicted rise time and measured data. In reality the increment of instability of the distortion modes is higher than follows from the presented theory. The dashed line in Figure 2 is obtained by letting $\lambda_1 = 6 \cdot 10^{-3}\omega_*$. This gives better agreement with the data. One should point out that the location of the threshold curve (see Figure 1) is very sensitive to the precision of satisfaction of resonant conditions $|\omega_p - \omega_*| \ll \omega_p$, $|\sigma_l - \omega_p/2| \ll \omega_p$. At the exact resonance $\omega_p = \omega_*$, $\sigma_l = \omega_p/2$ the lowest threshold amplitude is equal to $P_{th} \approx 23$ Pa and corresponding value of λ_1 (at 50 Pa) is equal to $\lambda_1 \approx 20 \cdot 10^{-3}\omega_*$. Thus the likeliest origin for this discrepancy is in the limited precision with which the threshold was determined. Certainly the published data shows that the threshold can be lower than the values used for the numerical calculations. The greater the amount by which the pump signal amplitude (here, 50 Pa) exceeds the threshold, the greater λ_1. Increasing λ_1 in the above calculation reduces the discrepancy. This does not validate the theory, but shows that to test it properly, the threshold needs to be known very accurately.

The end-point of the current paper is a comparison of theory with the existing experimental dataset. Given the limitations of the dataset, further experimentation is required. This is not only to determine the experimental parameters with greater precision (which, as was shown above), is necessary if a meaningful comparison with theory is to be made). It is also required because the existing literature suggests possible dependencies. First, the threshold might be influenced by the nature of the gas and liquid ("...the shape- distorting oscillations of bubbles are significantly affectedby the physical properties of both liquid and bubble gas"; [31]). Second, bubble surface oscillations are known to be very sensitive to the presence of surface contaminants [32, 33]. Third, the experiments have required the bubbles to be tethered by fine wire, or held under surfaces, which might lead to shape and acoustic effects that are not currently incorporated into the theory. Other developments to the theoy include consideration of the third order nonlinearity that alone can explain the appearance of regular structures in parametrically generated Faraday's ripples, observed on bubble walls. The final question is one of accounting for the near resonance interaction $(\sigma_l/\sigma_n)^2 \approx (\text{integeer})^2$ between shape distortion modes. It is correct to ignore this interaction in our case when one considers $l \gg 1$ and accounts for the quadratic nonlinearity (in this case the resonance condition is reduced to $\sigma_l \approx 2\sigma_n$). For $l = 11$ $(\sigma_{11}/2\sigma_7) \approx 0.03$, but the coupling constant that is proportional to the corresponding 3j symbol is small due to the relatively large discrepancy between $l = 11$ and $n = 7$. That is not the case when one can excite only first spherical harmonics $l = 2, 3 \ldots$ The coupling constant for the near resonance interaction is a unity on the order of magnitude as $l = 3$ close to $n = 2$ and this process plays an important role in energy transfer [31, 20].

7. Conclusions

In the present work the problem of parametrically driven bubble shape oscillations has been given full consideration, accounting for all spherical harmonics corresponding to $(2l+1)$ degenerate resonant surface modes. The derived theory can explain the significant difference, which has been experimentally observed, in the ring up times taken to establish subharmonic and fundamental combination frequency signals. The suggested explanation is based on the fact that the observed discrepancy takes place near the threshold for excitation of distortion modes, where the growth of an instability is very slow, which leads to a very long duration transient interval while establishing steady state surface oscillations.

Acknowledgement

The authors are thankful to the reviewer for helpful suggestions, particularly with regards to the direction for future work.

References

[1] T. Benjamin, M. Strasberg: Excitation of oscillations in the shape of pulsating bubble - theoretical work (a), - experimental work (b). J. Acoust. Soc. Am. **30** (1958) 697.
[2] D. Storm: Thresholds for surface waves and subharmonics associated with a single bubble. J. Acoust. Soc. Am. **522** (1972) 152.
[3] C. Hullin: Pulsierende Luftblasen in Wasser. Acustica **27** (1977) 64–72.
[4] D. Hsieh: On threshold for surface waves and subharmonics of an oscillating bubble. J. Acoust. Soc. Am. **56** (1974) 392–393.
[5] A. Francescutto, R. Nabergoj: Pulsation amplitude threshold for surface waves on oscillating bubbles. Acustica **41** (1978) 215–220.

[6] M. Ceschia, R. Nabergoj: On the motion of a nearly spherical bubble in a viscous liquid. Phys. Fluids. **221** (1978) 140–141.
[7] H. Rath: On the stability of gas bubble oscillating non spherically in a compressible liquid. Journ. of Engineering Math. **15** (1981) 161–170.
[8] P. Hall, G. Seminara: Nonlinear oscillations of non-spherical cavitation bubbles in acoustical fields. J. Fluid. Mech. **101** (1986) 423–444.
[9] M. Longuet-Higgins: Monopole emission of sound by asymmetric bubble oscillations. Part 1. Normal modes. J. Fluid Mech. **201** (1989) 525–541.
[10] M. Longuet-Higgins: Monopole emission of sound by asymmetric bubble oscillations. Part 2. An initial value problem. J. Fluid Mech. **201** (1989) 543–565.
[11] J. Ffowcs Williams, Y. Guo: On resonant nonlinear bubble oscillations. J. Fluid Mech. **224** (1991) 507–529.
[12] M. Longuet-Higgins: Resonance in nonlinear bubble oscillations. J. Fluid Mech. **224** (1991) 531–549.
[13] C. Mei, X. Zhou: Parametric resonance of a spherical bubble. J. Fluid Mech. **229** (1991) 229–250.
[14] S. Yang, Z. Feng, L. Leal: Nonlinear effects in dynamics of shape and volume oscillation for a gas bubble in an external flow. J. Fluid Mech. **247** (1993) 417–454.
[15] Z. Feng, L. Leal: Energy transfer mechanism in coupled bubble oscillations. Phys. Fluids A **5** (1993) 826–836.
[16] Z. Feng, L. Leal: Bifurcations and chaos in shape and volume oscillations of a periodically driven bubble with two-to-one internal resonance. J. Fluid Mech. **266** (1994) 206–242.
[17] Z. Feng, L. Leal: Translational instability of a bubble undergoing shape oscillations. Phys. Fluids A **7** (1995) 1325–1336.
[18] Z. Feng, L. Leal: Nonlinear bubble dynamics. Annu. Rev. Fluid Mech. **29** (1997) 201–247.
[19] M. Kornfeld, L. Suvorov: On the destructive action of cavitation. J. Appl. Phys. **15** (1944) 495–506.
[20] E. Trinh, D. Thiessen, R. Holt: Driven and freely decaying nonlinear shape oscillations of drops and bubbles immersed in a liquid: experimental results. J. Fluid Mech. **364** (1998) 253–272.
[21] G. Hansen: Mie scattering as a technique for the sizing of air bubbles. Appl. Opt. **24** (1985) 3214–3220.
[22] T. Asaki, P. Marston, E. Trinh: Shape oscillations of bubbles in water driven by modulated ultrasonic radiation pressure: Observation and detection with scattering laser light. J. Acoust. Soc. Am. **93** (1993) 706–713.
[23] T. Leighton, R. J. Lingard, A. Walton, J. Field: Acoustic bubble sizing by combination of subharmonic emissions with imaging frequency. Ultrasonics **29** (1991) 319–323.
[24] A. Phelps, T. Leighton: High-resolution bubble sizing through detection of the subharmonic response with a two-frequency excitation technique. J. Acoust. Soc. Am. **99** (1996) 1985–1992.
[25] A. Maksimov: On the subharmonic emission of gas bubble under two frequency excitation. Ultrasonics **35** (1997) 79–86.
[26] D. Ramble, A. Phelps, T. Leighton: On the relation between surface waves on a bubble and the subharmonic combination-frequency emission. Acustica - acta acustica **84** (1998) 986–988.
[27] M. Longuet-Higgins: Nonlinear damping of bubble oscillations by resonant interaction. J. Acoust. Soc. Am. **91** (1992) 1414–1422.
[28] S. Wiggins: Introduction to applied nonlinear dynamical systems and chaos. Springer Verlag, New York, 1996.
[29] H. Haken: Advanced synergetics. Springer-Verlag, Berlin, 1983.
[30] G. Korn, T. Korn: Mathematical handbook for scientists and engineers. McGraw-Hill, New York, 1961.
[31] T. J. Asaki, P. L. Marston: Free decay of shape oscillations of bubbles acoustically trapped in water and sea water. J. Fluid Mech. **300** (1995) 149–167.
[32] T. J. Asaki, D. B. Thiessen, P. L. Marston: Effect of an insoluble surfactant on capillary oscillations of bubble in water: Observation of a maximum in the damping. Phys. Rev. Lett. **75** (1995) 2686–2689.
[33] T. J. Asaki, P. L. Marston: The effect of a soluble surfactant on quadrupole shape oscillations and dissolution of air bubble in water. J. Acoust. Soc. Am. **102** (1997) 3372.